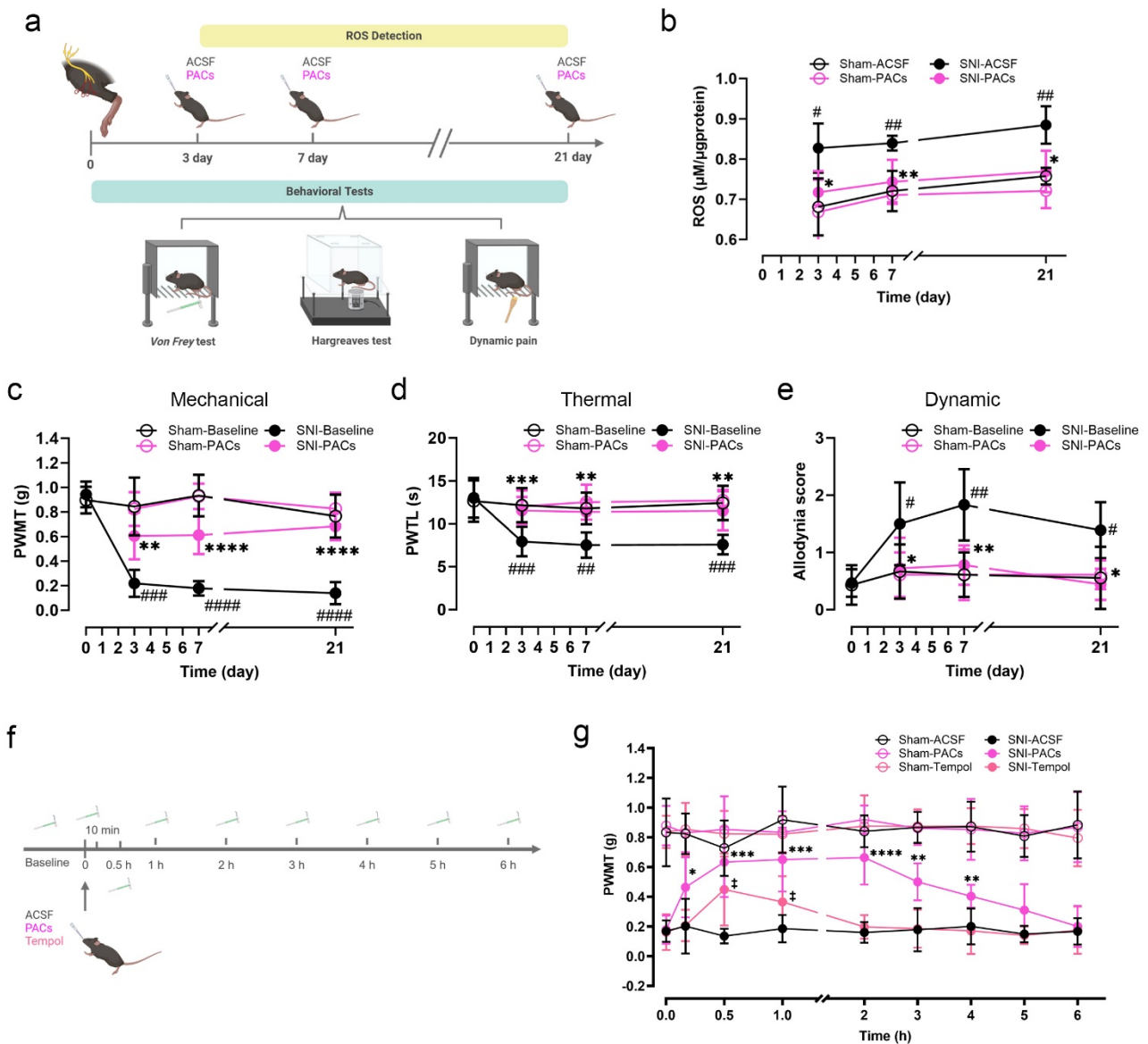Supplementary Fig. 1. Temporal changes in pain behaviors, ROS levels, and PACs' analgesic effects. a, Experimental timeline and setup for ROS detection and pain behavioral tests. **b**, Quantification of ROS levels in the VLO over time, with measurements taken at day 3, 7, and 21 post-surgery in sham and SNI mice. **c-e**, Temporal changes in pain behaviors following SNI and PACs treatment: **c**, Mechanical pain sensitivity (PWMT) measured by *von Frey* test at days 3, 7, and 21 post-surgery; **d**, Thermal pain sensitivity (PWTL) measured by Hargreaves test at day 3, 7, and 21 post-surgery; **e**, Dynamic allodynia score measured by brushing the lesioned paw at day 3, 7, and 21 post-surgery. **f**, Timeline for assessing the duration of analgesic effects of PACs and Tempol at 7 days post-surgery using the *von Frey* test. **g**, Time course of PWMT measurements following

intranasal administration of PACs or Tempol, showing changes in pain threshold over a 6-hour period. Data are expressed as mean ± S.D. #: sham-ACSF *vs.* SNI-ACSF, *: SNI-PACs *vs.* SNI-ACSF, ‡: SNI-Tempol *vs.* SNI-ACSF $^{*/\#/\ddagger}P < 0.05$, $^{**/\#\#}P < 0.01$, $^{***/\#\#\#}p < 0.001$, $^{****/\#\#\#\#}p < 0.0001$. See source data file for detailed statistical tests.

a
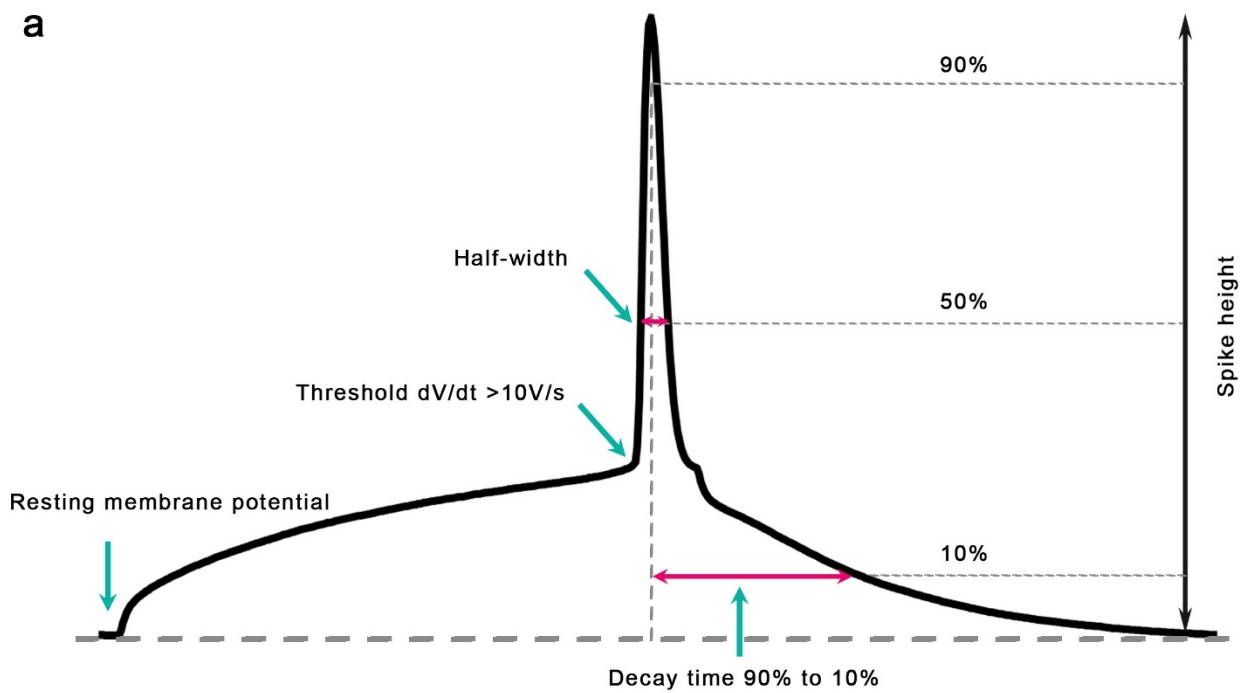
b

	Sham-Baseline	Sham-PACs	SNI-Baseline	SNI-PACs
AP threshold (mV)	-36.05 ± 0.5545	-36.93 ± 1.324	-39.58 ± 0.9157**	-37.97 ± 0.6133
Spike Height (mV)	114.1 ± 1.497	111.2 ± 1.674	114.3 ± 1.540	112.6 ± 1.658
Half- Width (ms)	1.861 ± 0.09948	1.920 ± 0.1380	1.535 ± 0.05326**	1.535 ± 0.05154
Rise time (ms)	0.2983 ± 0.01340	0.3156 ± 0.01702	0.2608 ± 0.005592*	0.2840 ± 0.009428
Max Rise slope (V/s)	188.5 ± 11.50	171.6 ± 13.43	209.7 ± 5.976	186.9 ± 7.300##
Max Decay slope (V/s)	-59.34 ± 3.707	-59.26 ± 4.591	-74.22 ± 2.892**	-74.27 ± 2.373
Decay time 90%to 10% (ms)	22.23 ± 1.487	24.11 ± 2.237	17.89 ± 1.367*	22.03 ± 1.743##

Supplementary Fig. 2. Summary of the electrophysiological parameters of AP of PYR^{VLO} in sham and SNI mice. a, A diagram displaying the electrophysiological parameters of AP elicited by rheobase current. **b,** Summary of the AP parameters of PYR^{VLO} in sham and SNI mice. Data are expressed as mean ± S.E.M. *: SNI-Baseline (n = 14) *vs.* Sham-Baseline (n = 14), two-tailed unpaired t test; #: SNI-PACs *vs.* SNI-Baseline, n = 14, two-tailed paired t test. */#$P < 0.05$, **/##$P < 0.01$.
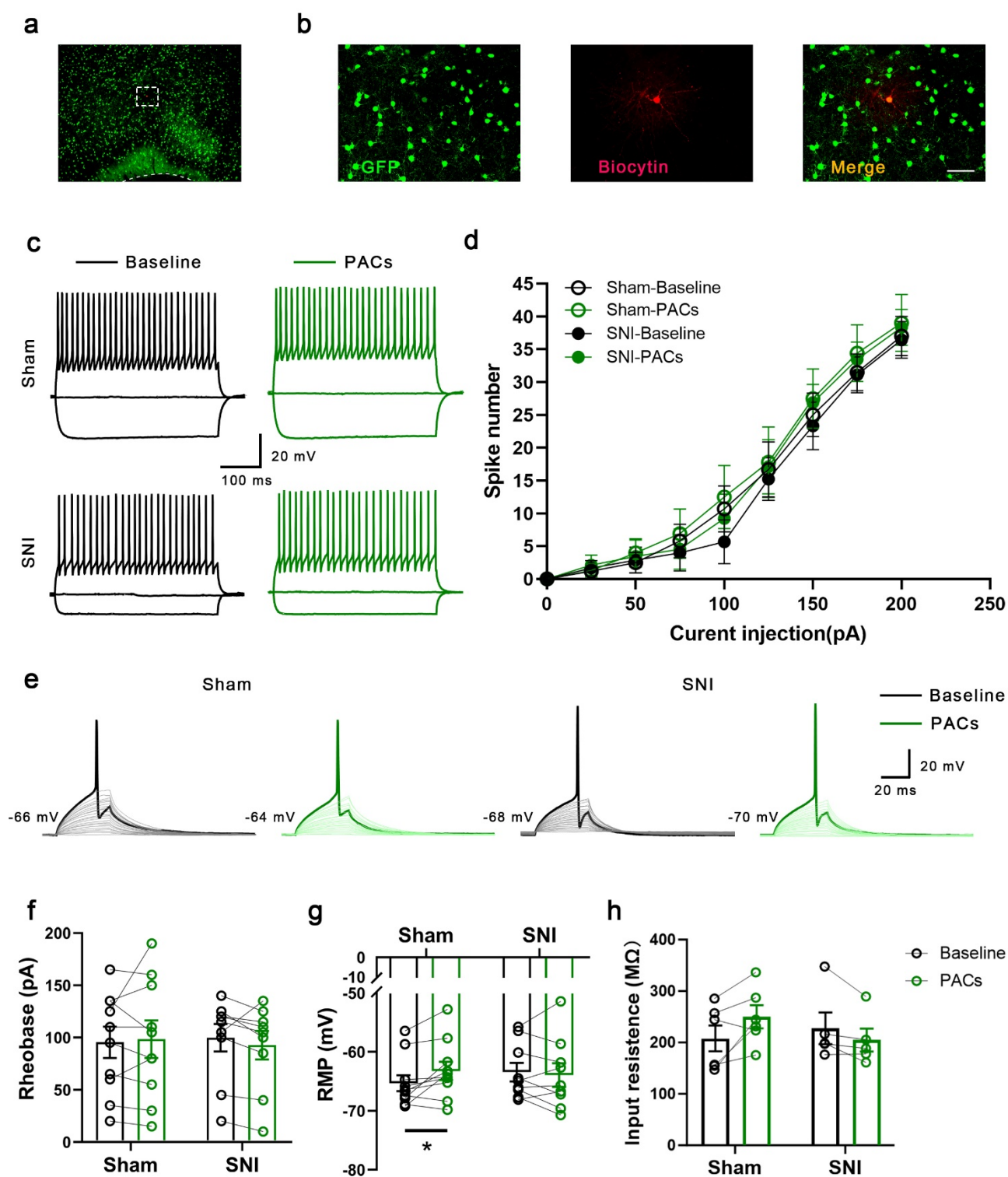
Supplementary Fig. 3. PACs have minimal impact on the activities of INT^{VLO}. a, GFP$^+$ neurons in the VLO in a GAD67-GFP transgenic mouse. **b,** Images showing GFP$^+$ interneurons (left), one whole-cell patched neuron labeled with biocytin and stained with TRITC (middle), and the merged image (right). **c,** Representative traces of action potentials elicited by 150 pA current stimulation before and during PACs application in sham

and SNI mice. **d**, Spikes evoked by step depolarizing currents before and during PACs application in sham (n = 10) and SNI (n = 9) mice. **e**, Representative traces of current threshold (rheobase) to elicit the first action potential before and during application of PACs in sham and SNI mice. **f**, Rheobase of INT^{VLO} before and during application of PACs in sham (n = 10) and SNI (n = 9) mice. **g**, RMP of INT^{VLO} before and during application of PACs in sham (n = 10) and SNI (n = 9) mice (Sham-Baseline *vs.* Sham-PACs, $p = 0.0268$). **h**, Input resistance of INT^{VLO} before and during application of PACs in sham (n = 6) and SNI (n = 5) mice (Sham-Baseline *vs.* Sham-PACs, $p = 0.0190$). Data are expressed as mean ± S.E.M. See source data file for detailed statistical tests. $*p < 0.05$.
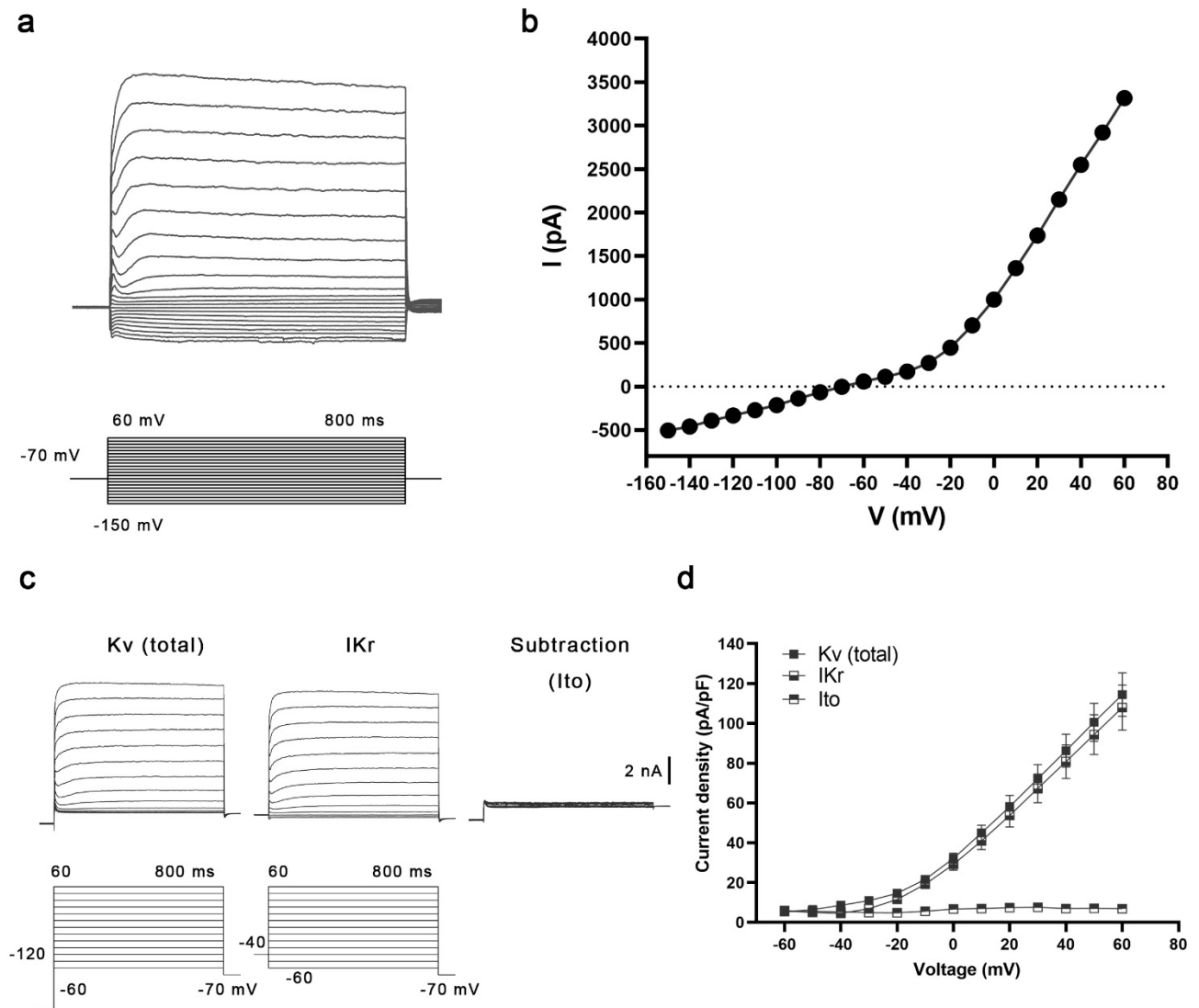
Supplementary Fig. 4. The delayed outward rectifier potassium current (Ikr) is the main component in the total voltage-dependent potassium (Kv) currents in PYR[VLO]. a, Representative traces of total potassium currents (top) and the voltage command (bottom). **b**, I-V curve of total potassium currents for (a). **c**, Representative traces of total voltage-dependent potassium (Kv) current (left), delayed outward rectifier potassium (Ikr) current (middle), and transient outward potassium (Ito) current (right) obtained by subtraction Ikr from total Kv. **d**, Current density-voltage curves for total Kv, Ikr and Ito. Data are expressed as mean ± S.E.M. n = 8. See source data file for detailed statistical tests.
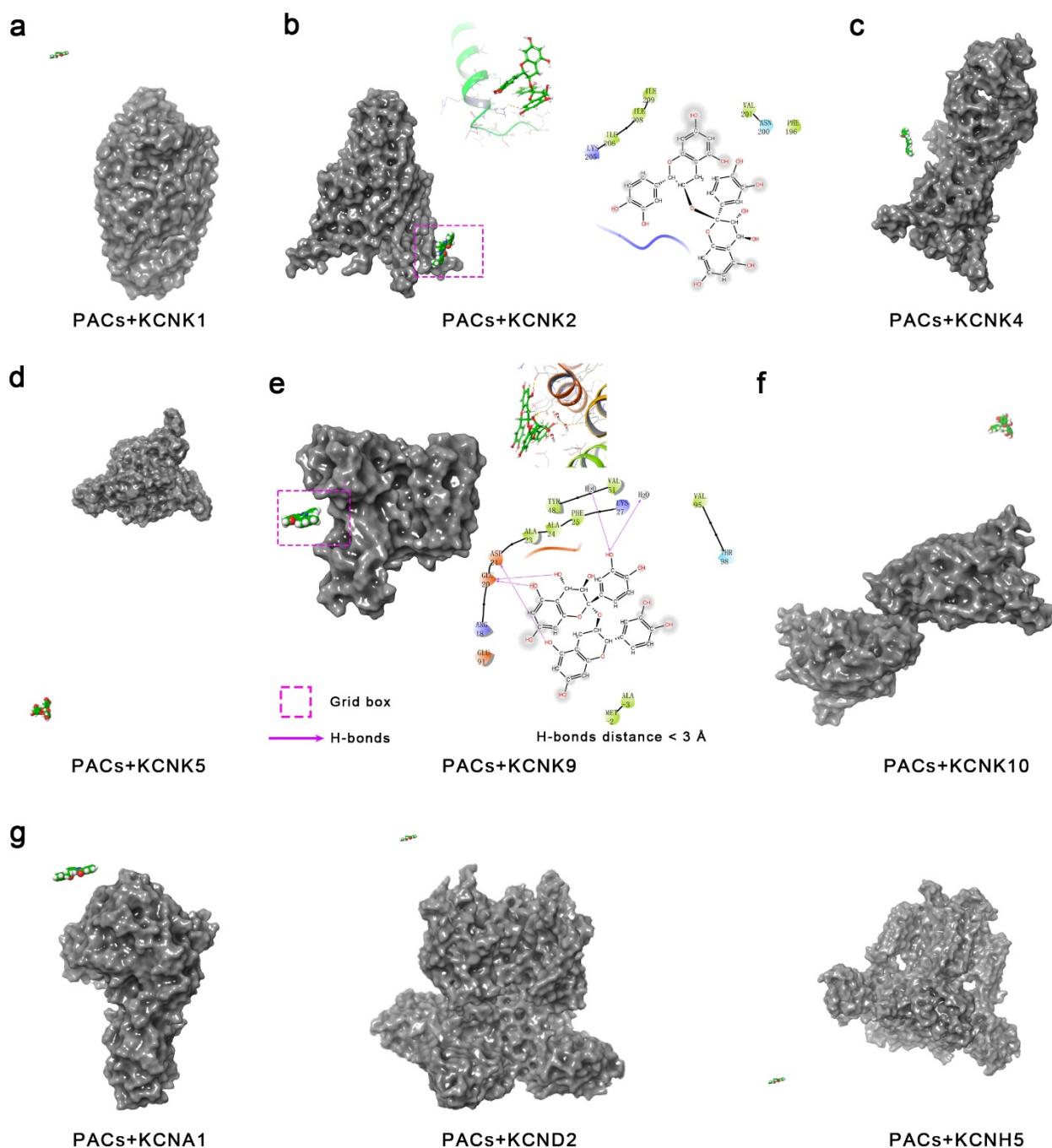
Supplementary Fig. 5. Prediction of PACs binding sites in other leak potassium channels and the PACs-downregulated Kv channels. a, PACs has no predicted binding site in KCNK1. **b**, The predicted binding site of PACs in KCNK2 is on the cytoplasmic domain. **c**, PACs has no predicted binding site in KCNK4. **d**, PACs has no predicted binding site in KCNK5. **e**, The predicted binding site of PACs in KCNK9 is on the transmembrane domain. **f**, PACs has no predicted binding site in KCNK10. **g**, PACs has no predicted binding sites in the

upregulated Kv channels in SNI mice.
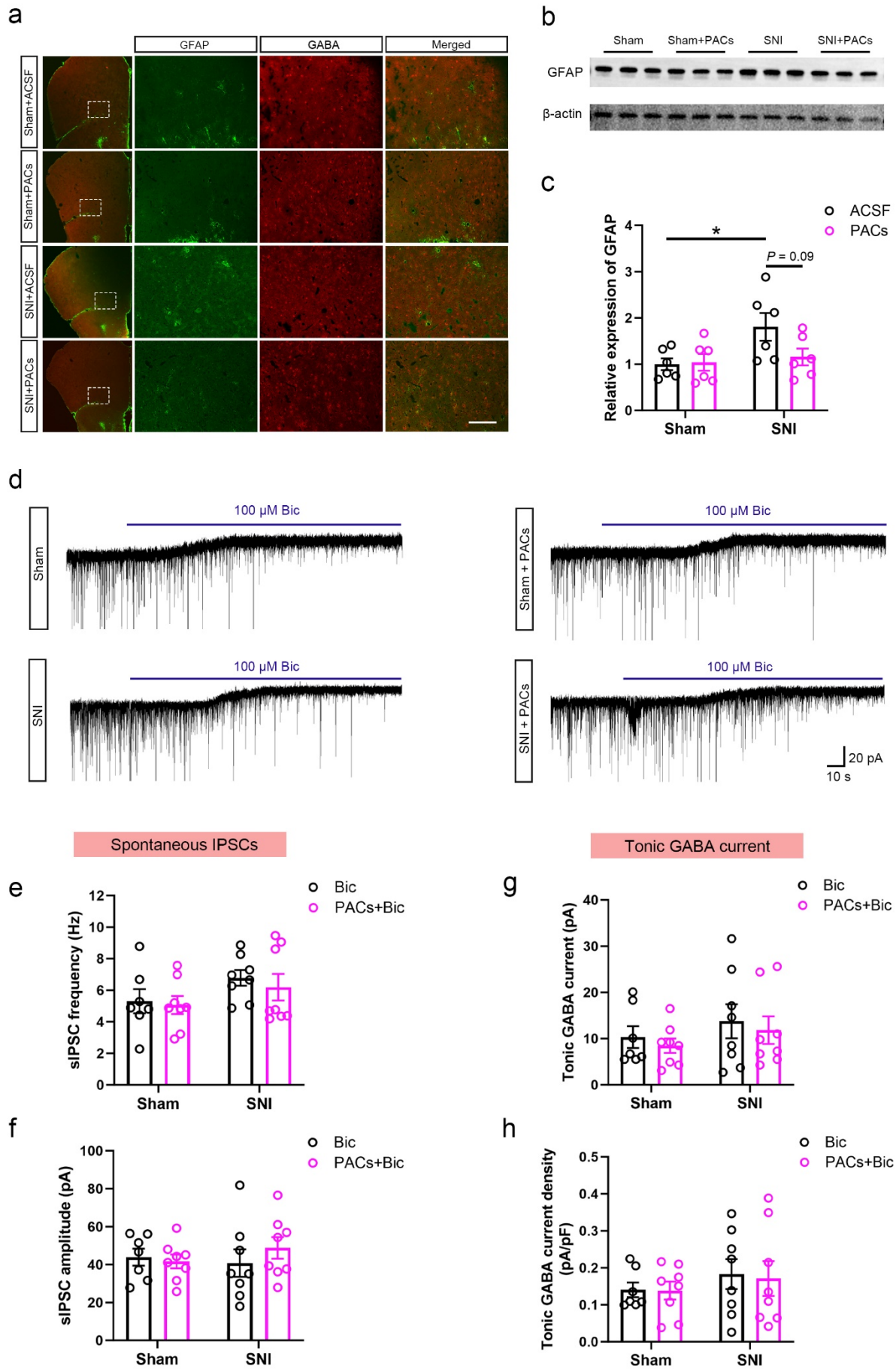
Supplementary Fig. 6. Astrocytes are activated after SNI, but PACs have no effect on the astrocytic GABA-mediated current. a, Immunofluorescence staining of GFAP (green) and GABA (red) in the VLO across different treatment groups. Scale bar = 100 µm. **b**, Western blot analysis of GFAP protein expression in the VLO across treatment groups, with β-Actin as the loading control. **c**, Summary data of relative GFAP expression levels: sham-ACSF (n = 6) vs. SNI-ACSF (n = 6), p = 0.0328. **d**, Representative traces of spontaneous IPSCs and tonic GABA-mediated current recorded in PYR^{VLO} in sham and SNI mice. **e-f**, summary data of frequency (**e**) and amplitude (**f**) of spontaneous IPSCs in Sham and SNI groups with and without PACs treatment. **g-h**, summary data of amplitude (**g**) and current density (**h**) of tonic GABAergic current in Sham and SNI groups with and without PACs treatment. Bic, bicuculline; sIPSC, spontaneous inhibitory postsynaptic currents. Data are expressed as mean ± S.E.M. *$P < 0.05$. See source data file for detailed statistical tests.